Optical Phonon Modes in Rectangular Graphene Quantum Dots

Jun Qian,[1] Mitra Dutta,[1,2] and Michael A. Stroscio[1,2,3,*]

[1]*Department of Electrical and Computer Engineering, University of Illinois at Chicago, Chicago, IL 60607 USA*
[2]*Department of Physics, University of Illinois at Chicago, Chicago, IL 60607 USA*
[3]*Department of Bioengineering, University of Illinois at Chicago, Chicago, IL 60607 USA*

(Received April 12, 2010)

Recently, graphene has been studied extensively as a promising material for future high-performance electronics. Dimensionally-confined graphene nanostructures are building blocks of devices and the carrier-phonon interactions in these device structures are frequently critical to their electronic properties. For a two-dimensional confined graphene nanosheet with orthogonal in-plane boundaries along armchair and zigzag edge, the confined carrier and optical phonon states are determined. The electron-longitudinal optical (LO)-phonon interactions in these graphene quantum dots are studied by the optical deformation potential theory. Phonon bottleneck effects are found for general graphene quantum dots. Carrier-LO-phonon scattering events are allowed only for graphene quantum dots with certain sizes; Fermi golden rule transition rates are evaluated approximately for cases where the dot dimensions are such that transitions are allowed.

PACS numbers: 63.22.Rc, 72.80.Vp, 73.22.Pr

I. INTRODUCTION

Graphene is a promising material for next-generation electronic devices as a result of its unique electronics properties [1–3], including high carrier mobility. Both carrier and phonon states need to be carefully considered in confined graphene nanostructures, such as nanoribbons [4–7] and quantum dots [8, 9]. At high temperature, carrier-phonon scattering dominates the carrier transport in moderately doped unconfined graphene samples [5, 10]. Thus, in order to provide a basis for both graphene-based electronics as well as modeling phonon modes and carrier-phonon interactions in graphene-based nanostructures, confined carrier states and confined long-wavelength phonon modes are considered herein for two-dimensional confined graphene nanostructures. For graphene confined in two dimensions, phonon bottleneck effects are found in this work. Forward or backward carrier-phonon scattering depends strongly on the dimensions of the graphene nanostructures and are calculated using Fermi's golden rule. These results are obtained by quantum confinement effects included using previous models for graphene-based structures [4, 7, 11–14].

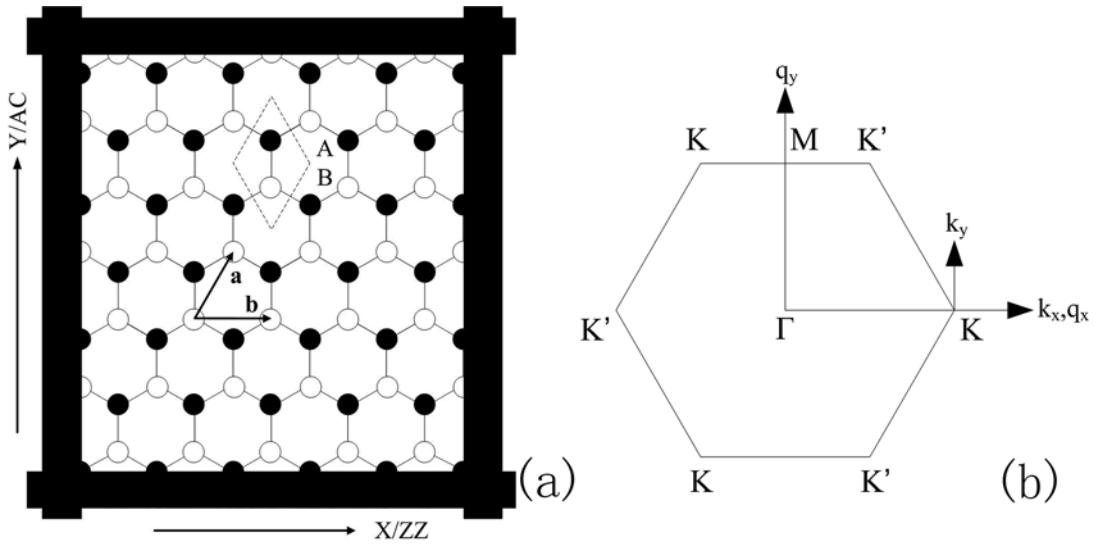

FIG. 1: (a) Rectangular graphene quantum dot model in infinite barriers, where filled and open circles are two sets of sublattice A and B, **a** and **b** are unit vectors, and dot line rhombic is the unit cell. (b) The reciprocal lattice, phonon of q_x and $q_y$is considered around the Γ point, while carrier of k_x and $k_y$is considered near K and K′ point.

II. THEORY

The rectangular graphene quantum dot (RGQD) model is given as Figure 1. The graphene nanosheet are confined with two externally defined orthogonal boundaries along the zigzag (ZZ) and armchair (AC) edges, which are referred as the x- and y-axis with M units and N units, respectively. The boundaries are treated as infinite barriers in the extreme quantum limit. Sublattice A (filled circles) are sublattice B (open circles) lie separately on ZZ edge and both on AC edges. The length of the ZZ edge, L_{ZZ}, is Ma, and the AC edge, L_{AC}, is $\left(N+\frac{1}{3}\right)\frac{\sqrt{3}}{2}a$, where $a = 2.46$ Å is the nearest distance between the two carbon atoms in the same sublattice. In Figure 1(b) is the reciprocal lattice, where the length of nearest neighbor inequivalent Dirac points KK' is $K_0 = 4\pi/3a$. The K point is $(K_0, 0)$, and the K′ point is $(-K_0, 0)$. Carrier states are considered near K and K′ points, while the phonon states are considered around the zone center, Γ point.

II-1. Double Quantized Carrier States in RGQD

The carrier states in RGQD are studied by the effective mass approximation [4, 15], which is reasonable to be adopted since we are interested in the low-energy carrier states near the K and K′ Dirac points. The total wavefunction of the sublattice A and B is written

as

$$\begin{cases} \Psi_A(\mathbf{r}) & = e^{i\mathbf{K}\cdot\mathbf{r}}\psi_A(\mathbf{r}) + e^{i\mathbf{K}'\cdot\mathbf{r}}\psi_A(\mathbf{r}) \\ \Psi_B(\mathbf{r}) & = e^{i\mathbf{K}\cdot\mathbf{r}}\psi_B(\mathbf{r}) + e^{i\mathbf{K}'\cdot\mathbf{r}}\psi_B(\mathbf{r}) \end{cases} \tag{1}$$

The Dirac Hamiltonian around the Dirac point K and K′ in momentum space ignoring the intervalley scattering [2] is given as

$$H_K = \hbar\nu_F \begin{pmatrix} 0 & k_x - ik_y \\ k_x + ik_y & 0 \end{pmatrix} \text{ and } H'_K = \hbar\nu_F \begin{pmatrix} 0 & k_x + ik_y \\ k_x - ik_y & 0 \end{pmatrix} \tag{2}$$

where $\nu_F = \sqrt{3}at/2 \approx 10^6$ m/s is the Fermi velocity at the Dirac points, $t(\approx 2.8$ eV) is the nearest-neighbor hopping energy [1], and k_x and k_y are the small wavevector perturbations from K or K′ point. The carrier energy is given as $\varepsilon = \pm\hbar\nu_F|k| = \pm\dfrac{\sqrt{3}ta}{2}\sqrt{k_x^2 + k_y^2}$, where $+$ is for electrons and $-$ for holes. The K and K′ valleys contribute independently to the conductivity when the intervalley scattering is neglected. The hard wall boundary conditions are applied for ZZ edge and AC edge [4, 5]. For the sake of convenience, only the carrier states near K point are considered for solution.

For ZZ edge along the x axis, the boundary conditions (located at $y = 0$ and $y = L_{AC}$) are given as $\Psi_A(y = 0) = 0$ and $\Psi_B(y = L_{AC}) = 0$, and for AC edge along the y axis, the boundary conditions (located at $x = 0$ and $x = L_{ZZ}$) are given as $\Psi_A(x = 0) = \Psi_A(x = L_{ZZ}) = 0$ and $\Psi_B(x = 0) = \Psi_B(x = L_{ZZ}) = 0$. Solve the Dirac equation, the solutions are given as

$$\begin{cases} \psi_A & = Ze^{ik_x x}\sin(k_y y) \\ \psi'_A & = -Ze^{-ik_x x}\sin(k_y y) \end{cases} \text{ and } \begin{cases} \psi_B & = Ze^{ik_x x}\sin(\theta_k + k_y y) \\ \psi'_B & = -Ze^{-ik_x x}\sin(\theta_k + k_y y) \end{cases} \tag{3}$$

where $\theta_k = \arctan(k_y/k_x)$, k_x and k_y around the K point need to satisfy

$$\begin{cases} (K_0 + k_x)L_{ZZ} & = m_k\pi \\ \theta_k + k_y L_{AC} & = n_k\pi \end{cases} \tag{4}$$

where m_k and n_k are integers showing the nature of quantized states. Z is the normalization constant determined by the normalization condition of $\displaystyle\int d\mathbf{r}\left[\left|\psi_{A,B}(\mathbf{r})\right|^2 + \left|\psi'_{A,B}(\mathbf{r})\right|^2\right] = \frac{1}{2}$, and it is given as

$$Z = \left[2L_{ZZ}L_{AC} + \frac{L_{ZZ}}{k_y}\sin(2\theta_k)\right]^{-1/2} = \left[2L_{ZZ}L_{AC} - \frac{L_{ZZ}}{k_y}\sin(2L_{AC}k_y)\right]^{-1/2} \tag{5}$$

which depends on both the electron states and the dimensions of the 2D-confined graphene nanosheet.

II-2. Confined Phonon Modes in RGQD and Deformation Potential Hamiltonian

The long-wavelength phonon dispersion is studied by means of an elastic continuum model, and by treating graphene nanosheet as a macroscopic 2D thin elastic sheet with negligible thickness [7, 12, 13]. This continuum model is expected to be most accurate for long wavelength modes; accordingly, this study focuses on the lowest order confined modes which correspond to the longest wavelength modes. The equation of motion for optical phonon modes are applied for the relative continuous displacement $\mathbf{U} = \mathbf{u_A} - \mathbf{u_B}$ of a 2D graphene sheet that are invariant under symmetry operations of the 2D graphene sheet [7]. Within the RGQD model, the solutions for double quantized phonon are given in the travelling wave form $\mathbf{U}(x, y, t) = \mathbf{A} \exp\Big[i\big(q_x x + q_y y - \omega t\big)\Big]$. The in-plane vibrations, u and ν, are correlated with each other, and the in-plane vibrations, u and ν, are decoupled with out-of-plane vibration, ω.

Since clamped boundaries conditions are assumed, the lattice displacements at the boundaries are all equal to zero. We will have the quantization condition [16, 17] for ZZ- and AC edges as

$$q_m = q_x = \frac{m_q \pi}{L_{ZZ}} \quad \text{and} \quad q_n = q_y = \frac{n_q \pi}{L_{AC}} \tag{6}$$

where m_q and n_q are integers. Thus, the dispersion curves of double quantized TO and LO phonons in RGQD are reproduced as

$$\begin{cases} \left(\omega_{mn}^{TO}\right)^2 = \omega_{TO}^2 - \beta_T^2 \left(q_m^2 + q_n^2\right) & \text{TO} \\ \left(\omega_{mn}^{LO}\right)^2 = \omega_{TO}^2 - \lambda^2 \left(q_m^2 + q_n^2\right)^2 + \beta_L^2 \left(q_m^2 + q_n^2\right) & \text{LO} \end{cases} \tag{7}$$

The parameters $(\beta_L, \beta_T, \lambda)$ are approximated by fitting the dispersion curves of LO and TO phonons in 2D graphite in the Γ-M direction [13] and have the values $\beta_L = 7.8 \times 10^5$ cm/s, $\beta_T = 9.6 \times 10^5$ cm/s, and $\lambda = 9.3 \times 10^{-3}$ cm^2/s; these constants represent the longitudinal and transverse sound speeds as well as the coefficient for the first higher order dispersion, respectively.

To calculate electron-LO phonon scattering, first the LO mode is normalized by the quantum-mechanical energy principle applied to the classical elastic modes [11]; then the optical deformation potential Hamiltonian can be determined from those normalized continuum modes [18] as

$$H_{opt-def} = D \cdot \mathbf{U} = |D|(u + \nu) \tag{8}$$

where D, the optical phonon deformation constant, is equal to 8.89 eV/Å [19]. For LO phonon mode, using the method in part 3 in ref. [7], we have

$$\begin{cases} u(x, y) &= u_0 \sin(q_m x) \sin(q_n y) \\ \nu(x, y) &= -\frac{q_n}{q_m} u_0 \sin(q_m x) \sin(q_n y) \end{cases} \tag{9}$$

The quantized displacement amplitudes, u_0 and ν_0 are

$$u_0 = \mu_{mn}^{LO} \sin\theta_q \qquad \text{and} \qquad \nu_0 = -\mu_{mn}^{LO} \cos\theta_q. \tag{10}$$

Thus the (m_q, n_q)-LO phonon deformation potential Hamiltonian is given as

$$H_{mn}^{LO} = |D|\mu_{mn}^{LO}(\sin\theta_q - \cos\theta_q)\sin(q_m x)\sin(q_n y) \tag{11}$$

where $\mu_{mn}^{LO} = \sqrt{\dfrac{2\hbar}{M\omega_{mn}^{LO}}}$, $\theta_q = \arctan(q_m/q_n)$, where $M = \rho L_{ZZ} L_{AC}$ is the total mass of the graphene nanosheet, and $\rho \approx 7.6 \times 10^{-7}$ kg/m^2 is the 2D mass density of single layer graphene.

II-3. Electron-LO phonon scattering rates

To evaluate the confined electron-phonon scattering rates, we use the deformation potential approximation and Fermi's golden rule for the intravalley electron-phonon scattering when considering perfect graphene quantum dots [2],

$$\Gamma^{\{e,a\}}(\mathbf{k}^f, \mathbf{k}^i) = g_\nu \frac{2\pi}{\hbar} \left| M^{\{e,a\}} \right|^2 \rho(E^f) \tag{12}$$

where $g_\nu = 2$ is the valley degeneracy degree, e and a represent emission and absorption, f and i designate the final and initial states, $M^{\{e,a\}}$ is the matrix element, and $\rho(E^f)$ is the density of final states. The matrix element is given as

$$M^{\{e,a\}}(q) = \sqrt{N_q + \frac{1}{2} \pm \frac{1}{2}}|D|\mu_{mn}^{LO}(\sin\theta_q - \cos\theta_q) \cdot Z^i Z^f A_\pm B_\pm \tag{13}$$

where $N_q = 1\left(e^{\hbar\omega_{LO}/k_B T} - 1\right)$ is the Bose-Einstein distribution; the upper and lower sign stands for emission and absorption, respectively, and

$$A_\pm = \pm\frac{i}{2} L_{ZZ} \text{ and } B_\pm = \frac{\sin\theta_k^i + \sin\theta_k^f}{4}\left(\frac{\sin\theta_k^f}{k_y^f} - \frac{\sin\theta_k^i}{k_y^i}\right) \mp \frac{\sin(\theta_k^i - \theta_k^f)}{4} L_{AC} \tag{14}$$

During the electron and phonon scattering, momentum conservation is

$$\pm q_x = k_x^i - k_x^f \qquad \text{and} \qquad \pm\, q_y = k_y^i - k_y^f. \tag{15}$$

For these double quantized electron and phonon states in a perfect RGQD, the only possibilities for conserving momentum correspond to the plus and minus signs in Eq. 15. The energy conservation in the scattering process can be written as

$$\Delta\varepsilon = \frac{\sqrt{3}at}{2}(k^f - k^i) = \mp\hbar\omega_{LO} \tag{16}$$

where $\Delta k = k^f - k^i$: when $\Delta k < 0$, a phonon is emitted, and $\Delta k > 0$, a phonon is absorbed.

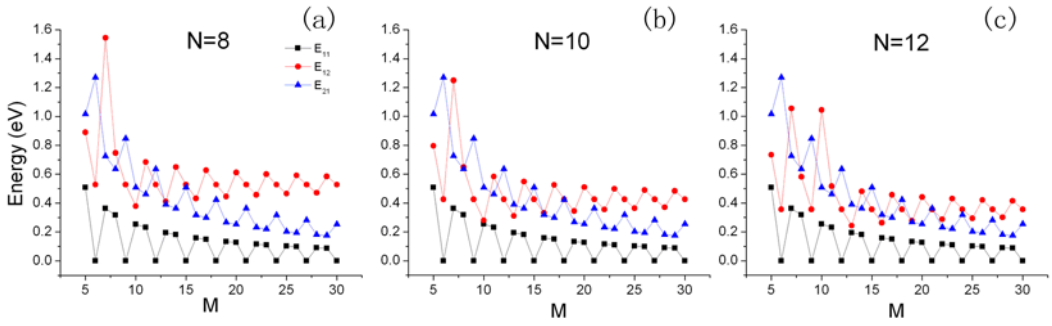

FIG. 2: The lowest three energy states of RGQD with varied L_{ZZ} or M and fixed L_{AC} or N equal (a) 8; (b) 10; (c) 12. The square, circle and up-triangle dots correspond to $(1,1)$, $(1,2)$ and $(2,1)$ energy states, respectively.

III. RESULT

The lowest three energy states, $(1,1)$, $(1,2)$ and $(2,1)$, are considered for carrier phonon scattering since they have the largest scattering rates. The energy states are complicated and needs to be carefully considered for each case of discrete dimensions. Figure 2 shows these energy states varied with M from 5 to 30 of fixed N equal to 8, 10 and 12. Generally, the RGQD of $M = 3M_0$ is metallic with zero $(1,1)$ energy state as shown in Figure 2. The $(1,1)$ and $(2,1)$ energy levels have the same properties for the three types of graphene nanosheets. For metallic RGQD, the $(2,1)$ energy states have higher energy than the two neighbor cases with $M = 3M_0 \pm 1$. These lowest three energy states decrease with increasing M. For large M, the energy states of certain N approach the same value agreeing with the 1D case of graphene nanoribbon. For small M, the $M = 3M_0 + 1$ graphene nanosheet is of complicated energy states since it depends on both M and N: when M is small, there exists abnormal large energy states for M equals 7 for N equals 8 and 10 and M equals 7 and 10 for N equals 12 and 10. The energy states of RGQD are quite sensitive to the ZZ and AC edge dimensions. Even with one period changing of the length, the electrical properties will change vastly.

Phonon bottleneck exists in general RGQD since the carrier and phonon states are discrete and hard to be matched with each other mimic to the cases of 3D quantum dots [20]. The RGQD with M and N equal to 8 is considered as an example, the size of which is 1.97 nm for ZZ edge and 1.78 nm for AC edge. Figure 3(a) shows the discrete energy levels of the electrons with certain k_x and k_y near the K point in the first quadrant, where the other three quadrants are mirror symmetry to the first quadrant. The lowest three energy levels are 0.317 eV for $(1,1)$, 0.635 eV for $(2,1)$, and 0.747 eV for $(1,2)$. With larger M and N, i.e., longer ZZ- and AC edges, the discrete energy levels will become closer with higher density and become quasi-continuous when M and N are large enough. The discrete energy states of LO phonon are shown in Figure 3(b) with the maximum energy 0.196 eV of state $(2,3)$. Generally, the energy of the lowest few LO phonon modes are taken

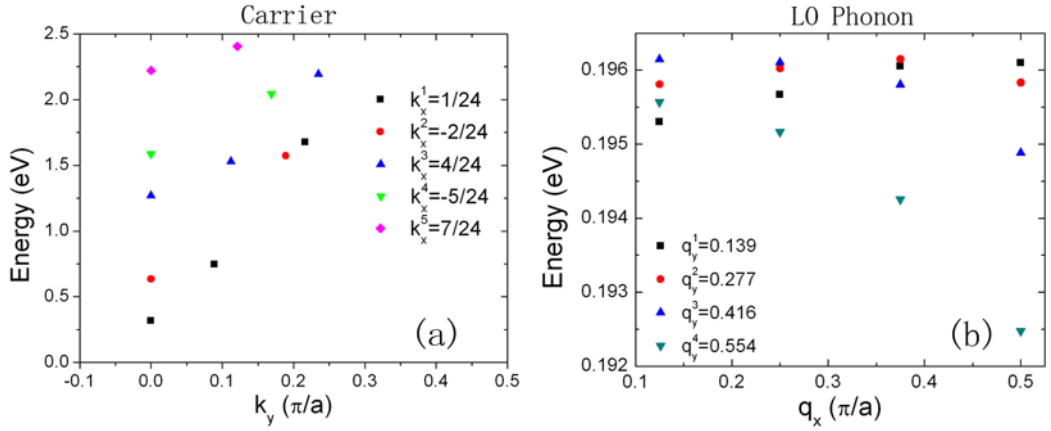

FIG. 3: (a) The carrier states and (b) LO phonon states of RGQD with $M = N = 8$ for zigzag and armchair edges. The quantized wavevectors k_x, k_y, q_x and q_y are all in unit π/a.

as 0.195 eV in the long wavelength approximation. Carefully comparing the energy and momentum difference between the two electron states in Figure 3(a) with the quantized LO phonon states in Figure 3(b), no strictly matched electron states and LO phonon modes can be found. Similarly do the TO phonon modes. Since the RGQD is confined in all the dimensions just like 3D quantum dots, there are no continuous wavevectors for the 2D-clamped graphene nanosheets.

To strictly satisfy the momentum conservation and energy conservation as Eq. 15 and 16, respectively, we need to carefully choose the dimensions of the RGQD. Considering the lowest phonon mode — the $(1, 1)$ phonon mode — which generally has the largest scattering rate, the dimensions of the quantum-dot should satisfy $\frac{1}{L_{AC}^2} + \frac{1}{L_{ZZ}^2} = \frac{1}{9.61^2}$ nm^{-2} in order to conserve energy and momentum. Considering graphene nanosheets with appropriate scales, we calculated the scattering rates at room temperature for both phonon emission and absorption events involving the scattering of the lowest $(1, 1)$ LO phonon. When M and N are 77 and 52, forward scattering is allowed with phonon emission and absorption rates of 1.063 ps^{-1} and 5.23×10^{-3} ps^{-1}, respectively. At room temperature, the absorption scattering rate is negligible for low energy carriers; while for carriers of large energy, the LO phonon emission dominates. The emission and absorption scattering rates are very sensitive to the length of the ZZ edge, which decreases to 1.732×10^{-3} ps^{-1} and 8.54×10^{-6} ps^{-1} even for just one period variation from $M = 77$ to 76. This also elucidates that the phonon bottleneck effect generally occurs except for some special dimensions. For backward scattering, the phonon emission and absorption scattering rates are 7.99 ps^{-1} and 3.93×10^{-3} ps^{-1}, respectively, when M and N are 26 and 17. For forward scattering, the dimensions of ZZ and AC edges are quite large compared with the examples given in Figures 2 and 3, which is reasonable since the sizes of the graphene nanosheet need to be large enough so that the energy difference between two nearest energy levels becomes

comparable to the LO phonon energy. The dimensions for backward scattering are much smaller than those of forward scattering since they can provide larger momentum difference.

IV. DISCUSSION AND CONCLUSIONS

Phonon bottleneck effects exist widely in nanostructures with all dimensional confined, such as quantum dots [20–22] and short carbon nanotubes [14, 23]. Generally, the phonon bottleneck effect is predicted to exist in most cases of RGQDs due to the discrete nature of the electron states and thus the mismatch of the electronic energy gaps with the discrete LO phonon modes. The electron-LO phonon scattering, which usually dominates at high temperature in carbon nanotube, can be ruled out in general RGQDs cases, thus the total electron relaxation rates will be vastly lowered. Thus, it is expected that there will be enhanced quasi-ballistic transport in 2D confined graphene nanosheets similar to what is found for short carbon nanotube transistors [24]. Phonon bottleneck's another evident is the vastly reduce of the scattering rate caused by the small variation of the dimensions due to the picky size conditions for both energy and momentum conservations.

However, when applying our model to the real cases, we have two limits to be noticed. First, when the scale of the graphene nanosheet is large, the energy levels become quasi-continuous. It is reasonable to question our model's validity for such large-scale cases when the 2D confined graphene nanosheet should be treated as continuous graphene nanoribbon or bulk sheet. Another limit is that the infinite barrier assumption does not work in real cases, which may disturb the scattering rates of these of extreme quantum limits. Also, it is hard to testify the phonon bottleneck effect discussed in the paper due to the limitation of current fabrication technology, which is very difficult to fabricate atomic-smooth-edge graphene nanostructure. In the real graphene nanostructures with rough edge, one of the other important scattering mechanisms is the interference (IF) phonons, which need to be especially considered for device applications with confined electrodes. Also, the edge roughness scattering [25] may be the other dominant factor, and obviously, it is not considered in our model.

In summary, we studied double quantized electron states by effective mass method and double confined optical phonon modes through elastic continuum model in RGQD. Phonon bottleneck effect is predicted to exist in most cases of RGQDs. Only the forward and backward intravalley electron-LO phonon scatterings are allowed in certain RGQDs with special dimensions, where the scattering rates are calculated using Fermi's golden rule. These calculations predict a larger backscattering rate in smaller graphene quantum dot. It is expected that the phonon bottleneck effect will vastly lower the scattering rate due to the elimination of the electron-LO phonon scattering mechanism.

Acknowledgments

J. Q. acknowledges the support of the China Scholarship Council. Special thanks are given to Prof. Jean-Pierre Leburton of UIUC for enlightening comments.

References

* Electronic address: stroscio@uic.edu

[1] A. H. Castro Neto, F. Guinea, N. M. R. Peres, *et al.*, Reviews of Modern Physics **81**, 109–162 (2009).
[2] K. Nomura and A. H. MacDonald, Physical Review Letters **98**, 076602 (2007).
[3] M. I. Katsnelson, K. S. Novoselov, and A. K. Geim, Nature Physics **2**, 620–625 (2006).
[4] L. Brey and H. A. Fertig, Physical Review B **73**, 235411 (2006).
[5] T. Fang, A. Konar, H. Xing, *et al.*, Physical Review B **78**, 205403 (2008).
[6] D. Gunlycke, H. M. Lawler, and C. T. White, Physical Review B **75**, 085418 (2007).
[7] J. Qian, M. J. Allen, Y. Yang, *et al.*, Superlattices and Microstructures **46**, 881–888 (2009).
[8] L. A. Ponomarenko, F. Schedin, M. I. Katsnelson, *et al.*, Science **320**, 356–358 (2008).
[9] B. Wunsch, T. Stauber, and F. Guinea, Physical Review B **77**, 035316 (2008).
[10] F. Rana, P. A. George, J. H. Strait, *et al.*, Physical Review B **79**, 115447 (2009).
[11] A. Raichura, M. Dutta, and M. A. Stroscio, Superlattices and Microstructures **35**, 147–153 (2004).
[12] H. Suzuura and T. Ando, Physical Review B **65**, 235412 (2002).
[13] S. V. Goupalov, Physical Review B **71**, 085420 (2005).
[14] A. Raichura, M. Dutta, and M. A. Stroscio, Physica Status Solidi B-Basic Research **241**, 3448–3453 (2004).
[15] T. Ando, Journal of the Physical Society of Japan **74**, 777–817 (2005).
[16] S. Kitipornchai, X. Q. He, and K. M. Liew, Physical Review B **72**, 075443 (2005).
[17] J. Atalaya, A. Isacsson, and J. M. Kinaret, Nano Letters **8**, 4196–4200 (2008).
[18] M. A. Stroscio, M. Dutta, D. Kahn, *et al.*, Superlattices and Microstructures **29**, 405–409 (2001).
[19] A. Akturk, G. Pennington, N. Goldsman, *et al.*, IEEE Transactions on Nanotechnology **6**, 469–474 (2007).
[20] R. M. Delacruz, S. W. Teitsworth, and M. A. Stroscio, Superlattices and Microstructures **13**, 481–486 (1993).
[21] R. Heitz, H. Born, F. Guffarth, *et al.*, Physical Review B **64**, 241305(R) (2001).
[22] O. V. Prezhdo, Chemical Physics Letters **460**, 1–9 (2008).
[23] M. Steiner, M. Freitag, V. Perebeinos, *et al.*, Nature Nanotechnology **4**, 320–324 (2009).
[24] A. Javey, J. Guo, Q. Wang, *et al.*, Nature **424**, 654–657 (2003).
[25] F. Sols, F. Guinea, and A. H. Castro Neto, Physical Review Letters **99**, 166803 (2007).